Facile and Generalized Preparation of Hierarchically Mesoporous−Macroporous Binary Metal Oxide Materials

Zhong-Yong Yuan, Tie-Zhen Ren, Aurélien Vantomme,† and Bao-Lian Su*

Laboratory of Inorganic Materials Chemistry, The University of Namur (FUNDP), 61 rue de Bruxelles, B-5000 Namur, Belgium

Received March 26, 2004. Revised Manuscript Received September 2, 2004

A family of binary oxide compositions, including titania−zirconia, titania−alumina, alumina−zirconia, zirconia−silica, and alumina−silica, with a hierarchically bimodal mesoporous−macroporous structure has been prepared. The macropores are in one-dimensional orientation, parallel with each other, and the macroporous framework is composed of interconnected wormhole-like mesopores. The mesopore sizes of the binary oxides, as well as macropore sizes, could be tailored by the variation of the molar ratios of the metal precursors. The crystalline phase modification was observed in these binary oxides. The role of surfactant molecules in the creation of the porous hierarchy has been discussed. These meso−macroporous binary oxides show higher surface areas, larger pore volumes, and higher thermal stabilities than single metal oxides, exhibiting efficient potential of applications, especially in catalysis.

Introduction

The successful development of surfactant-templated synthesis of mesostructured inorganic/surfactant composites[1] has attracted many efforts in the conception of the ordered mesoporous transition metal oxides for their enormous potential in the fields of electromagnetics, photoelectronics, catalysis, and separation.[2] Mesoporous oxides of Ti,[3] Zr,[4] Nb,[5,6] Ta,[6] Al,[7] Sn,[8] Hf,[9] and Mn[10] have been synthesized using cationic, anionic, or neutral surfactants as structure-directing agents, although most of them were comprised of mainly amorphous framework walls, which would limit their thermal and hydrothermal stability and greatly compromise their usefulness in catalytic applications. Stucky et al. then synthesized mesoporous metal oxides with a semicrystalline framework by block copolymer templating.[11] Mesoporous aluminum oxide materials with crystalline AlOOH (boehmite) and γ-Al_2O_3 were demonstrated by Pinnavaia et al. using amine and PEO surfactants as structure directors, respectively.[12] Mesoporous titania with crystalline framework[13] and mesoporous crystalline β-FeOOH (akaganeite)[14] were also prepared recently.

Titania- and zirconia-based mixed oxides are of great importance due to their multiple applications, including catalysis and solid-oxide fuel cells.[15,16] It is known that the catalytic efficiency of metal oxides can be improved

* Corresponding author. Tel: +32-81-724531. Fax: +32−81−725414. E-mail: bao-lian.su@fundp.ac.be.

† FRIA fellow (Fonds National de la Recherche Scientifique, 5 rue d'Egmont, B-1000, Bruxelles, Belgium).

(1) Kresge, C. T.; Leonowicz, M. E.; Roth, W. J.; Vartuli, J. C.; Beck, J. S. *Nature* **1992**, *359*, 710.

(2) (a) He, X.; Antonelli, D. *Angew. Chem., Int. Ed.* **2002**, *41*, 214. (b) Schuth, F. *Chem. Mater.* **2001**, *13*, 3184. (c) Sayari, A.; Liu, P. *Microporous Mater.* **1997**, *12*, 149.

(3) (a) Antonelli, D. M. *Microporous Mesoporous Mater.* **1999**, *30*, 315. (b) Yoshitake, H.; Sugihara, T.; Tatsumi, T. *Chem. Mater.* **2002**, *14*, 1023. (c) Khushalani, D.; Ozin, G. A.; Kuperman, A. *J. Mater. Chem.* **1999**, *9*, 1491. (d) Trong, O. D. *Langmuir* **1999**, *15*, 8561. (e) Cabrera, S.; Haskouri, J. E.; Beltrán-Porter, A.; Beltrán-Porter, D.; Marcos, D. D.; Amorós, P. *Solid State Sci.* **2000**, *2*, 513. (f) Soler-Illia, G. J. A. A.; Louis, A.; Sanchez, C. *Chem. Mater.* **2002**, *14*, 750. (g) Putnam, R. L.; Nakagawa, N.; McGrath, K. M.; Yao, N.; Aksay, I. A.; Grunner, S. M.; Navrotsky, A. *Chem. Mater.* **1997**, *9*, 2690. (h) Antonelli, D. M.; Ying, J. Y. *Angew. Chem., Int. Ed. Engl.* **1995**, *34*, 2014.

(4) (a) Ciesla, U.; Schacht, S.; Stucky, G. D.; Unger, K. K.; Schüth, F. *Angew. Chem., Int. Ed. Engl.* **1996**, *35*, 541. (b) Ciesla, U.; Fröba, M.; Stucky, G.; Schüth, F. *Chem. Mater.* **1999**, *11*, 227. (c) Reddy, J. S.; Sayari, A. *Catal. Lett.* **1996**, *38*, 219. (d) Knowles, J. A.; Hudson, M. J. *J. Chem. Soc., Chem. Commun.* **1995**, 2083. (e) Hudson, M. J.; Knowles, J. A. *J. Mater. Chem.* **1996**, *6*, 89; f) Blin, J. L.; Flamant, R.; Su, B. L. *Inter. J. Inorg. Mater.* **2001**, *3*, 959. (g) Pacheco, G.; Zhao, E.; Garcia, A.; Sklyarov, A.; Fripiat, J. J. *Chem. Commun.* **1997**, 491. (h) Wong, M. S.; Ying, J. Y. *Chem. Mater.* **1998**, *10*, 2067. (i) Ulagappan, N.; Raju, V. N.; Rao, C. N. R. *Chem. Commun.* **1996**, 2243. (j) Huang, Y. Y.; McCarthy, T. J.; Sachtler, W. M. H. *Appl. Catal. A* **1996**, *148*, 135. (k) McIntosh, D. J.; Kydd, R. A. *Microporous Mesoporous Mater.* **2000**, *37*, 281. (l) Antonelli, D. M. *Adv. Mater.* **1999**, *11*, 487.

(5) (a) Lee, B.; Lu, D. L.; Kondo, J. N.; Domen, K. *J. Am. Chem. Soc.* **2002**, *124*, 11256. (b) He, X.; Antonelli, D. M.; Trudeau, M. L. *Adv. Mater.* **2000**, *12*, 1036. (c) Murray, S.; Trudeau, M. L.; Antonelli, D. M. *Adv. Mater.* **2000**, *12*, 1339.

(6) (a) Antonelli, D. M.; Ying, J. Y. *Chem. Mater.* **1996**, *8*, 874. (b) Antonelli, D. M.; Ying, J. Y. *Angew. Chem., Int. Ed. Engl.* **1996**, *35*, 426. (c).

(7) (a) Bagshaw, S. A.; Pinnavaia, T. J. *Angew. Chem., Int. Ed. Engl.* **1996**, *35*, 1102. (b) Gonzalez-Pena, V.; Diaz, I.; Marquez-Alvarez, C.; Sastre, E.; Perez-Pariente, J. *Microporous Mesoporous Mater.* **2001**, *44*, 203. (c) Yada, M.; Machida, M.; Kijima, T. *Chem. Commun.* **1996**, 769. (d) Vaudry, F.; Khodabandeh, S.; Davis, M. *Chem. Mater.* **1996**, *8*, 1451. (e) Valange, S.; Guth, J. L.; Kolenda, F.; Lacombe, S.; Gabelica, Z. *Microporous Mesoporous Mater.* **2000**, *35*, 597. (f) Cabrera, S.; El Haskouri, J.; Alamo, J.; Beltran, A.; Bltran, D.; Mendioroz, S.; Marcos, M. D.; Amoros, P. *Adv. Mater.* **1999**, *11*, 379. (g) Deng, W.; Toepke, M. W.; Shanks, B. H. *Adv. Funct. Mater.* **2003**, *13*, 61.

(8) Severin, K. G.; AbdelFattah, T. M.; Pinnavaia, T. J. *Chem. Commun.* **1998**, 1471.

(9) Liu, P.; Liu, J.; Sayari, A. *Chem. Commun.* **1997**, 577.

(10) Tian, Z.; Tong, W.; Wang, J.; Duan, N.; Krishnan, V. V.; Suib, S. L. *Science* **1997**, *276*, 926.

(11) (a) Yang, P.; Zhao, D.; Margolese, D. I.; Chmelka, B. F.; Stucky, G. D. *Nature* **1998**, *396*, 152. (b) Yang, P.; Zhao, D.; Margolese, D. I.; Chmelka, B. F.; Stucky, G. D. *Chem. Mater.* **1999**, *11*, 2813.

(12) (a) Hicks, R. W.; Pinnavaia, T. J. *Chem. Mater.* **2003**, *15*, 78. (b) Zhang, Z.; Hicks, R. W.; Pauly, T. R.; Pinnavaia, T. J. *J. Am. Chem. Soc.* **2002**, *124*, 1592.

(13) (a) Ren, T. Z.; Yuan, Z. Y.; Su, B. L. *Chem. Phys. Lett.* **2003**, *374*, 170. (b) Luo, H. M.; Wang, C.; Yan, Y. S. *Chem. Mater.* **2003**, *15*, 3841.

(14) Yuan, Z. Y.; Su, B. L. *Chem. Phys. Lett.* **2003**, *381*, 710.

10.1021/cm0494812 CCC: $27.50
Published on Web 10/23/2004

by doping the metal oxide with a metal or combining it with another metal oxide.[17] Porous mixed oxides of TiO_2/ZrO_2 and TiO_2/In_2O_3 formed by a polymer gel templating technique exhibited higher photocatalytic activities in comparison with the solitary metal oxide.[18] Mesoporous yttria-stabilized zirconia (YSZ) has shown its superior candidacy for the development of improved performance solid oxide fuel cell electrode material.[19] Ordered cubic and hexagonal mesoporous yttria−zirconia and ceria−zirconia thin films with high thermal stability have also been synthesized by an evaporation-induced self-assembly of metal chlorides with templating of PEO-based block copolymer.[20] However, little work has been done on the preparation of hierarchically porous binary mixed oxides with ordering on multiple length scale.

By utilization of multimodal templating of polymeric latex spheres[21] and surfactant supramolecular assembly,[1,11] the transition-metal oxides with controlled multimodal porosity (macro-, meso-, and microdomains) could be obtained.[22] We have demonstrated a simple procedure for the synthesis of uniform mesoporous−macroporous metal oxide materials by single surfactant templating technique[23] without the need for polymeric spheres or vesicles[24] or emulsion drops[25] as a template for the macroporous structure generation. In this paper, we extend this method to the synthesis of meso−macroporous binary metal oxides. A family of binary oxide compositions, including titania−zirconia (TZ), titania−alumina (TA), alumina−zirconia (AZ), zirconia−silica (ZS), and alumina−silica (AS), with a hierarchically bimodal meso−macroporous structure was prepared through the surfactant templating technique combining with the use of mixed alkoxide solutions. The binary metal oxide materials obtained have a homogeneous distribution of the components and the attractive structural properties of large pore volume and high specific surface area. Such hierarchical porous materials should be significant to give improved catalytic efficiency, due to the presence of a secondary metal oxide and structural control,[18] and are capable as catalyst or catalyst support for one-pot reaction process design. The synthesis was performed in the presence of either cationic alkyltrimethylammonium or nonionic PEO surfactant, accessing the formation of bimodal meso−macroporous oxide composites with very high surface areas.

Experimental Section

Syntheses. Cetyltrimethylammonium bromide (CTAB), Brij 56 [$C_{16}(EO)_{10}$], zirconium propoxide, titanium isopropoxide, aluminum *sec*-butoxide, and tetraethyl orthosilicate are commercially available from Aldrich. All chemicals were used as received. In a typical synthesis of meso−macroporous TZ, a solution of CTAB or Brij 56 (15 wt %) was prepared by dissolving the surfactant in a H_2SO_4 aqueous solution of pH = 2. A mixture of zirconium propoxide and titanium isopropoxide with different metal-to-metal molar ratio (M_A/M_B) [the total metal content ($M = M_A + M_B$) was limited to surface/M ratio of 0.33) was added drop by drop into the above medium under stirring, followed by further stirring for 1 h. The obtained mixture was then transferred to a Teflon-lined autoclave and heated at 60 °C for 48 h under static condition. The surfactant species were removed by Soxhlet extraction with ethanol over 36 h. The recovered product was dried at 60 °C in a vacuum. Other mixed oxide compositions, TA, AZ, ZS, and AS, were synthesized with the above method at the aging temperature of 80 °C for 24 h by using aluminum *sec*-butoxide and tetraethyl orthosilicate as alumina and silica sources, respectively. Calcination process was carried out in a conventional muffle oven by increasing the temperature from room temperature to 500 °C at 1 °C/min and heating at 500 °C for 30 min.

Characterization. Low-angle and wide-angle X-ray powder diffraction (XRD) patterns were obtained on a Philips PW 1820 diffractometer using Cu Kα radiation. N_2 adsorption−desorption isotherms were determined on a Micromeritics Tristar 3000 system at liquid nitrogen temperature. The surface area was obtained by the Brunauer−Emmett−Teller (BET) method, and the pore size distribution was calculated from the adsorption branch of the isotherm by the Barret−Joyner−Halenda (BJH) model. Scanning electron microscopy (SEM) and transmission electron microscopy (TEM) were carried out with a Philips XL-20 at 15 keV and a Philips TECNAI-10 at 100 kV, respectively. The specimens for TEM observation were prepared by epoxy resin-embedded microsectioning and mounting on a copper grid. Fourier transform infrared spectrometry was carried out with a Perkin-Elmer Spectrum 2000 spectrometer. Solid-state ^{27}Al and ^{29}Si magic angle spinning (MAS) nuclear magnetic resonance (NMR) spectra were recorded on Bruker MSL-400 and Bruker AVANCE500 spectrometers operating at resonance frequencies of 104.3 and 99.4 MHz and pulses of 1.0 μs ($\theta = \pi/12$) and 4 μs ($\theta = \pi/6$) with repetition times of 0.2 and 6 s, respectively. Chemical shifts were referenced to tetramethylsilane for ^{29}Si and to $[Al(H_2O)_6]^{3+}$ for ^{27}Al.

Results

The synthesis of meso−macroporous metal oxides and mixed binary oxides was performed at 60−80 °C in the presence of surfactants of either cationic CTAB or nonionic Brij 56. Metal alkoxides were used as the inorganic precursors. Almost all of the surfactant species present in the product could be removed by ethanol extraction, as confirmed by the infrared spectroscopy. The synthesized zirconium oxides are uniformly meso−macrostructured, but the structural framework is amorphous (Figure 1). The zirconia particles are monolithic with the particle size of tens of micrometers, exhibiting uniform macropores of 300−600 nm in diameter, revealed by both SEM and TEM micrographs. The macrochannels are arranged parallel to each other and perpendicular to the tangent of the surface of the particle; the pores are funnel-like (tapered toward the

(15) Takahashi, T.; Minh, N. Q. *Science and Technology of Ceramic Fuel Cells*; Elsevier: New York, 1995.
(16) (a) Daturi, M.; Binet, C.; Lavalley, J. C.; Galtayries, A.; Sporken, R. *Phys. Chem. Chem. Phys.* **1999**, *1*, 5717. (b) Lai, S. Y.; Pan, W.; Ng, C. F. *Appl. Catal. B* **2000**, *24*, 207.
(17) Miller, J. B.; Ko, E. I. *Catal. Today* **1997**, *35*, 269.
(18) (a) Schattka, J. H.; Shchukin, D. G.; Jia, J.; Antonietti, M.; Caruso, R. A. *Chem. Mater.* **2002**, *14*, 5103. (b) Shchukin, D. G.; Schattka, J. H.; Antonietti, M.; Caruso, R. A. *J. Phys. Chem. B* **2003**, *107*, 952.
(19) (a) Mamak, M.; Coombs, N.; Ozin, G. A. *Adv. Mater.* **2000**, *12*, 198. (b) Mamak, M.; Coombs, N.; Ozin, G. A. *J. Am. Chem. Soc.* **2000**, *122*, 8932. (c) Mamak, M.; Coombs, N.; Ozin, G. A. *Adv. Funct. Mater.* **2001**, *11*, 59.
(20) Crepaldi, E. L.; Soler-Illia, G. J. de A. A.; Bouchara, A.; Grosso, D.; Durand, D.; Sanchez, C. *Angew. Chem., Int. Ed.* **2003**, *42*, 347.
(21) (a) Yang, P.; Deng, T.; Zhao, D.; Feng, P.; Pine, D.; Chmelka, B. F.; Whitesides, G. M.; Stucky, G. D. *Science* **1998**, *282*, 2244. (b) Blanford, C. F.; Yan, H.; Schroden, R. C.; Al-Daous, M.: Stein, A. *Adv. Mater.* **2001**, *13*, 401.
(22) Grosso, D.; Soler-Illia, G. J. de A. A.; Crepaldi, E. L.; Charleux, B.; Sanchez, C. *Adv. Funct. Mater.* **2003**, *13*, 37.
(23) (a) Blin, J. L.; Léonard, A.; Yuan, Z. Y.; Gigot, L.; Vantomme, A.; Cheetham, A. K.; Su, B. L. *Angew. Chem., Int. Ed.* **2003**, *42*, 2875. (b) Yuan, Z. Y.; Vantomme, A.; Léonard, A.; Su, B. L. *Chem. Commun.* **2003**, 1558.
(24) Antonelli, D. M. *Microporous Mesoporous Mater.* **1999**, *33*, 209.
(25) Yuan, Z. Y.; Ren, T. Z.; Su, B. L. *Adv. Mater.* **2003**, *15*, 1462.

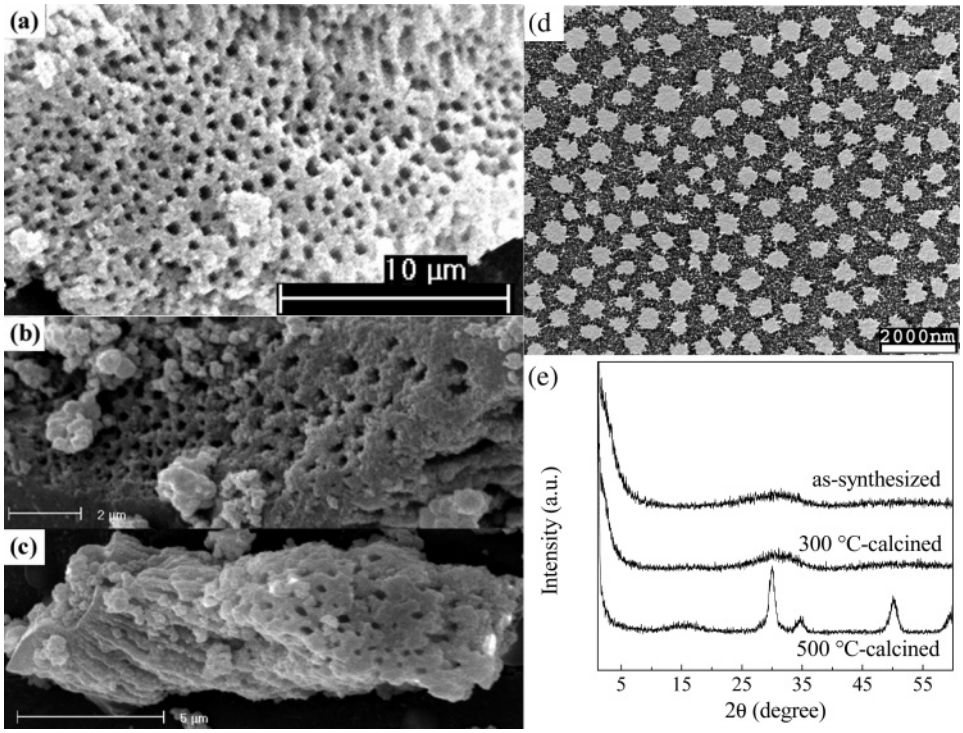

Figure 1. SEM images of the meso−macroporous zirconium oxides (a) as-synthesized and after calcinations at (b) 300 °C and (c) 500 °C; (d) the cross-sectional TEM image of the meso−macropore structure; and (e) XRD patterns of the zirconias before and after calcination.

center) in shape.[23] The macroporous framework is composed of accessible mesochannels with a wormhole-like array. The surface area of the synthesized zirconias could be up to 700 m^2/g.[23] Such a meso−macroporous structure could be retained after calcination at 300 °C (Figure 1b), and the surface area of about 300 m^2/g could be still obtained. However, calcination at 500 °C resulted in the reduction of the surface area to lower than 100 m^2/g, and the meso−macrostructures were somewhat partly deformed because of crystallization of the amorphous pore structure (Figure 1c), showing the poor thermal stability.

The as-synthesized meso−macroporous aluminum oxides were crystalline with the structural type of AlOOH (boehmite),[26] and the macropore size (0.8−2 μm) was larger than that of zirconia. After calcination at 500 °C, AlOOH was converted to γ-Al_2O_3 with the retention of the uniform meso−macrostructure. The TEM images of the boehmite and γ-Al_2O_3 specimens revealed that their macroporous frameworks were composed of fibrous nanoparticles of boehmite and γ-Al_2O_3 with a scaffold-like array of hierarchical ordering, respectively.[26] The mesostructures of boehmite and γ-Al_2O_3 were formed through the scaffold-like aggregation and intergrowth of the boehmite and γ-Al_2O_3 nanofibers, respectively. The BET surface areas of AlOOH and γ-Al_2O_3 were 381 and 424 m^2/g, respectively. The solid-state ^{27}Al MAS NMR spectrum of the meso−macroporous AlOOH (boehmite) contained only one single signal of six-coordinate Al species, and the spectrum of the γ-Al_2O_3 showed the presence of four- and six-coordinate Al in ~25:75 ratio. Little or almost no five-coordinate Al was observed for the meso−macroporous γ-Al_2O_3, signifying the absence of appreciable quantities of amorphous domains in the walls.[12]

The structural and textural properties of the meso−macrostructured single metal oxides could be improved by the introduction of secondary oxide to form the binary metal oxide composite materials. The general tendency is that the synthesized binary mixed oxides have higher surface areas than the single metal oxides. Moreover, not only the mesopore sizes, but also the macropore sizes of binary metal oxides could be tailored and controlled by the variation of the molar ratios of the metal precursors. The thermal stability of the binary oxide compositions could also be enhanced significantly. These meso−macrostructured binary oxide compositions should be significant for the use as advanced functional materials, especially in the catalysis applications.

Titania−Zirconia. SEM images revealed that the synthesized TZ samples made in the presence of either CTAB or Brij 56 surfactant are composed of particles with macroporous structures (Figure 2). A lot of particles are found to contain a macroporous array having diameters of 0.6−3 μm. A regular array of the macropores can clearly be seen. Interestingly, the macropore size increased with the TiO_2 content in the synthesized materials. Moreover, the macropores are usually of one-dimensional orientation, parallel to each other and orthogonal to one side of the monolithic particles. These well-oriented macrochannels extend through almost the whole particle. Such a macroporous structure was further confirmed by the TEM of the microtomed specimens (Figure 2d). It can be seen that the macropore sizes are not as homogeneously distributed as the pure zirconias. The wall thickness between the macropores with circular openings is around 0.3−3 μm. High-magnification TEM images of the cross-sectional TZ

(26) Ren, T. Z.; Yuan, Z. Y.; Su, B. L. *Langmuir* **2004**, *20*, 1531.

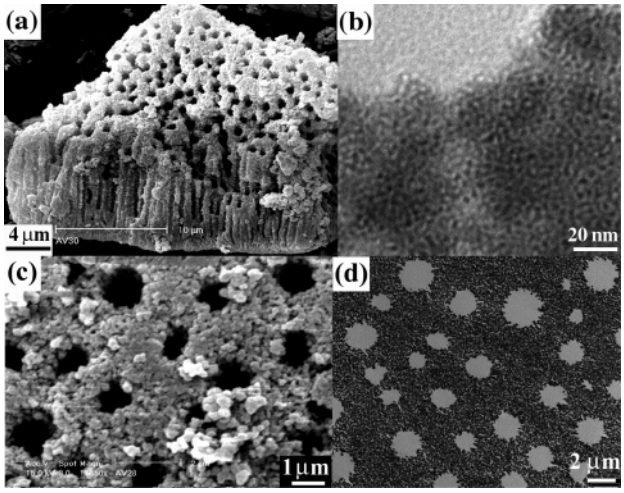

Figure 2. (a) SEM image of the meso–macroporous TZ composite with Ti/Zr = 5/5; (b) TEM image of the macropore walls of part a; (c) SEM image of the TZ composite with Ti/Zr = 8/2; and (d) cross-sectional TEM image of part c.

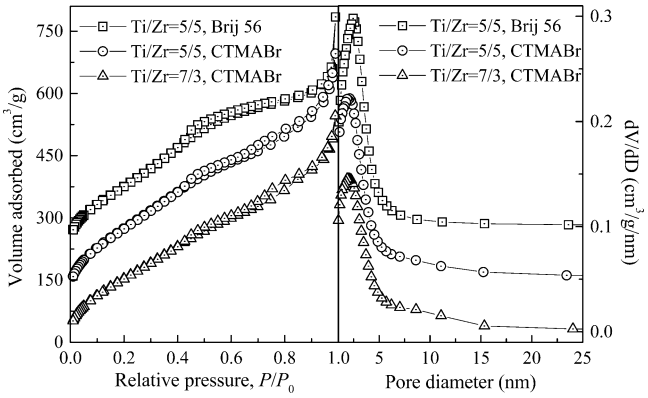

Figure 3. N_2 adsorption–desorption isotherms (left) of the meso–macroporous TZ samples as-synthesized with different surfactant and Ti/Zr ratio and their corresponding pore size distribution plots (right) obtained by the BJH method using the adsorption branch of the isotherms. The volume adsorbed was shifted by 100 and 200, and the d*V*/d*D* value was shifted by 0.05 and 0.10 for the curves of Ti/Zr = 5/5, CTMABr and of Ti/Zr = 5/5, Brij 56, respectively.

specimens also reveal that the macroporous frameworks are composed of nanoparticles with accessible and interconnected mesopores of a disordered wormhole-like array (Figure 2b).

Figure 3 shows representative nitrogen adsorption–desorption isotherms and the corresponding pore size distributions of the as-synthesized TZ composites. The increase in adsorbed volume at high relative pressure is a direct indication of the presence of the secondary large pores. In general, all the obtained TZ composite materials, whatever their Ti/Zr molar ratios in the synthesis gel, exhibit quite narrow pore size distribution peaks, indicative of the homogeneity of the mesoporosity of our materials, with higher surface areas and larger pore volumes than the pure titania and zirconia samples (Table 1). It is important that the mesopore size can be well adjusted by the variation of titania content in the composites.

Low-angle X-ray diffraction (XRD) patterns of these TZ samples gave a broad peak between 1° and 3° of 2θ, characteristic of a disordered mesostructure with no discernible long-range order in the mesopore arrangement.[27] The disordered mesostructure is consistent with TEM observations. The wide-angle XRD patterns of the TZs with different Ti/Zr ratios in the synthesis gel gave information about the crystalline phase of the inorganic materials (Figure 4). The TZ sample with a Ti/Zr ratio of 9/1 in the synthesis gel consists mainly of anatase titania crystals with traces of the brookite phase, which is similar to the pure titania sample, except the reduced intensity seen by XRD. The diffraction intensities of the anatase phase in the TZs decreased with the increase of the zirconia content. A further increase of the zirconia content inhibits crystallization, as no crystalline phase could be detected by XRD in the TZs with zirconia content above 50 mol %, indicating a homogeneous mixing of the Ti and Zr components in these materials. This suggests that the segregation did not occur, and meso–macrostructured TZs were formed with (Ti,Zr)-O_2 species, a real solid solution of TiO_2 and ZrO_2, rather than discrete TiO_2 and ZrO_2 nanocrystallites.

Table 1. Structural Properties of Some Synthesized Meso–Macroporous Binary Mixed Oxide Materials

surfactant	composition[a] (mol %) Ti	Zr	Al	Si	S_{BET} (m^2/g)	V_{pore} (cm^3/g)	D_{meso} (nm)	crystal phase[b]
CTMABr	–	100	–	–	593	0.502	1.8	(amorph)
CTMABr	50	50	–	–	720	0.922	2.2	(amorph)
CTMABr	70	30	–	–	632	0.845	2.0	An
CTMABr	80	20	–	–	595	1.014	3.4	An, trace of Br
CTMABr	90	10	–	–	213	0.597	5.6	An, trace of Br
Brij 56	50	50	–	–	704	0.904	2.5	trace of An
Brij 56	70	–	30	–	571	0.889	3.5	trace of An
Brij 56	50	–	50	–	893	1.573	2.8	(amorph)
Brij 56	30	–	70	–	557	0.968	2.6	trace of Bo
Brij 56	–	–	100	–	381	0.682	3.0	Bo
Brij 56	–	70	30	–	593	0.726	1.7	Ba
Brij 56	–	50	50	–	502	0.991	1.8	Ba
Brij 56	–	30	70	–	534	1.372	2.1	Ba, trace of Bo
Brij 56	–	–	70	30	574	1.454	7.1	trace of Bo
Brij 56	–	–	50	50	630	1.940	5.1	(amorph)
Brij 56	–	–	30	70	518	1.116	5.2	(amorph)
Brij 56	–	70	–	30	794	0.749	1.4	(amorph)
Brij 56	–	50	–	50	597	1.384	1.1	(amorph)
Brij 56	–	30	–	70	965	2.966	n.a.	(amorph)

[a] The composition content in the synthesis gel. [b] Abbreviations: An, anatase; Br, brookite; Bo, bohmite AlO(OH); Ba, bayerite $Al(OH)_3$; amorph, no peaks obtained in wide-angle XRD, indicating amorphous material.

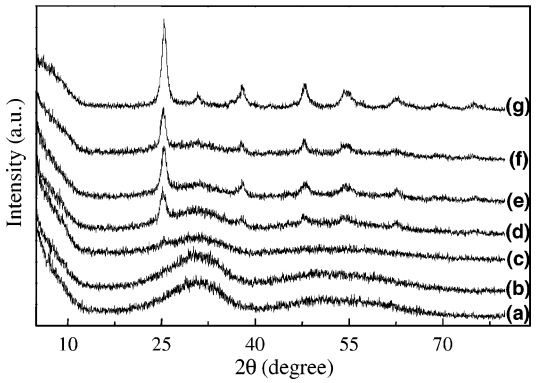

Figure 4. Wide-angle XRD patterns of the CTAB-templated titania–zirconia composites with different Ti/Zr ratios: (a) 100% ZrO_2; (b) 80% ZrO_2, 20% TiO_2; (c) 50% ZrO_2, 50% TiO_2; (d) 30% ZrO_2, 70% TiO_2; (e) 20% ZrO_2, 80% TiO_2; (f) 10% ZrO_2, 90% TiO_2; and (g) 100% TiO_2.

(27) Bagshaw, S. A.; Pinnavaia, T. J. *Angew. Chem., Int. Ed. Engl.* **1996**, *35*, 1102.

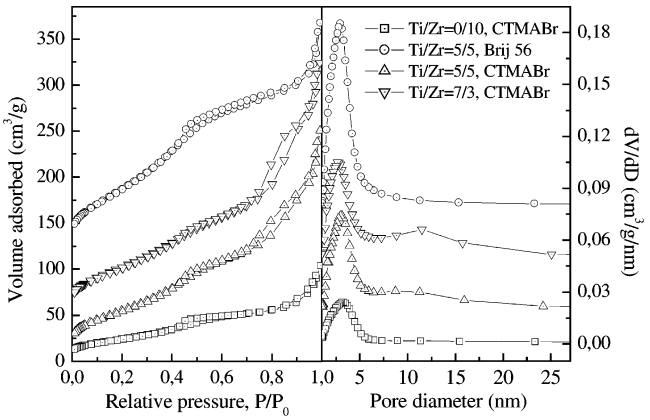

Figure 5. N_2 adsorption−desorption isotherms (left) and the corresponding BJH pore size distributions (right) of the TZ composites calcined at 500 °C. The volume adsorbed was shifted by 0, 40, and 100 and the d*V*/d*D* value was shifted by 0.02, 0.05, and 0.08 for the curves of Ti/Zr = 5/5, CTMABr, of Ti/Zr = 7/3, CTMABr, and of Ti/Zr = 5/5, Brij 56, respectively.

Table 2. Structural Properties of the Meso−Macroporous Binary Mixed Oxide Materials after Calcinations at 500 °C

	composition[a] (mol %)				S_{BET}	V_{pore}	D_{meso}	crystal
surfactant	Ti	Zr	Al	Si	(m^2/g)	(cm^3/g)	(nm)	phase[b]
CTMABr	−	100	−	−	90	0.161	3.1	teZ
CTMABr	50	50	−	−	205	0.388	3.1	teZ, An
CTMABr	70	30	−	−	232	0.440	2.8	An, teZ
Brij 56	100	−	−	−	125	0.212	5.5	An, trace of Br
Brij 56	50	50	−	−	327	0.414	3.0	trace of An, teZ
Brij 56	70	−	30	−	443	0.945	4.4	An
Brij 56	50	−	50	−	535	1.305	3.9	(amorph)
Brij 56	30	−	70	−	542	1.308	3.9	(amorph)
Brij 56	−	−	100	−	424	1.013	8.0	γ-Al_2O_3
Brij 56	−	70	30	−	289	0.409	1.75	(amorph)
Brij 56	−	50	50	−	287	0.631	1.63	(amorph)
Brij 56	−	30	70	−	349	1.036	1.7	(amorph)
Brij 56	−	−	70	30	367	1.093	7.2	(amorph)
Brij 56	−	−	50	50	380	1.267	5.1	(amorph)
Brij 56	−	−	30	70	448	1.138	∼5.3	(amorph)
Brij 56	−	70	−	30	302	0.283	1.4	(amorph)
Brij 56	−	50	−	50	470	0.926	1.7	(amorph)
Brij 56	−	30	−	70	758	1.840	n.a.	(amorph)

[a] The composition content in the synthesis gel. [b] Abbreviations: moZ, monoclinic ZrO_2 (baddeleyite); teZ, tetragonal ZrO_2; An, anatase; Br, brookite; amorph, no peaks obtained in wide-angle XRD, indicating amorphous material.

After calcinations at 500 °C, the pure zirconia presented tetragonal ZrO_2 crystals (Figure 1e), while the pure titania sample retained the same mixed phases of anatase and brookite but with the increased diffraction intensity. The bicrystalline phases of tetragonal ZrO_2 and anatase with low crystallinity were observed in the calcined TZs, and the diffraction intensity of the anatase phase decreased with the increase of the zirconia content in the samples, accompanying the increase of the diffraction intensity of the tetragonal ZrO_2 (Supporting Information). The meso−macrostructures can be retained after calcination, as revealed by SEM and TEM images. The N_2 adsorption−desorption isotherms and the corresponding pore size distributions of the calcined TZs are shown in Figure 5, and their textural properties are listed in Table 2. The pore sizes of the TZs were slightly enlarged after calcination. The BET surface areas and the pore volumes of the calcined TZs are larger than those of the calcined pure titania or zirconia (Table 2). The surface areas of the calcined TZs remain higher than 300 m^2/g, but the pure zirconia has a surface area of only 90 m^2/g after calcination at 500 °C, indicating the higher thermal stability of the TZ meso−macroporous materials.

Zirconia−Silica. Figure 6 shows the SEM images and N_2 adsorption−desorption isotherms of the synthesized ZS materials. A large number of tens-of-micrometer-sized monolithic particles with uniform macroporous structure are seen, and the macropores are parallel, running through the whole particles, which are in comparison with the macrostructures of the pure zirconias. The macroporous framework is amorphous, as revealed by the XRD patterns. A near vertical uptake of N_2 at low relative p/p_0 can be seen in the isotherms of the ZSs, indicating the presence of micropores (<2 nm). The BJH adsorption pore size distribution curves also confirm this tendency of the micropore size (Table 1). Thus, the present ZSs could be called micro−macroporous materials. Moreover, the micropore size of these ZSs significantly decreases with the increase of the silica content. The BET surface areas and pore volumes of the ZSs are larger than those of pure zirconia (Table 1). The ZS sample with a Zr/Si ratio of 3/7 in the synthesis gel shows the highest surface area of 965 m^2/g with a pore volume of 2.97 cm^3/g. It is noted that the specific surface areas determined by the BET method, based on the assumption of uniform monolayer−multilayer formation with the absence of micropores, may be overestimated for the hierarchical porous materials, and the alternative methods, such as the comparative method, are also effective for the evaluation of the surface areas. The BJH method might give underestimated pore size values, and some new interesting methods have been developed recently by Kruk et al.[28] We used the BET and BJH methods here for the sake of simplicity and systematic comparison, and the presented values are still informative.

After calcination at 500 °C, the uniform macroporous structure can be held without any deformation. The macroporous frameworks of these ZSs are still amorphous after this calcination (Supporting Information), indicating that the calcination-induced crystallization of zirconia has strongly been delayed by the doping of silica. This also suggests that no segregation of zirconia and silica took place in the meso−macroporous ZS composites. The surface areas of all the calcined ZSs were higher than those of the calcined pure zirconias and increased with the content of silica (Table 2). The micropore sizes slightly increased after calcination. A very high surface area of 758 m^2/g with pore volume of 1.84 cm^3/g can still be seen in the calcined ZS with a Zr/Si ratio of 3/7 in the synthesis gel.

Alumina−Silica. Figure 7 shows the XRD patterns of the as-synthesized and calcined meso−macroporous AS materials with different Al/Si ratios. The as-synthesized meso−macroporous pure aluminum oxide is crystalline with the structural type of AlOOH (boehmite) (Figure 7a),[26] and its calcined form is the γ-Al_2O_3 structure (Figure 7e). However, the modified crystalline structures can be seen in the AS composites. The crystalline phases of the as-synthesized ASs varied from

(28) (a) Kruk, M.; Antochshuk, V.; Jaroniec, M.; Sayari, A. *J. Phys. Chem. B* **1999**, *103*, 10670. (b) Kruk, M.; Jaroniec, M. *Chem. Mater.* **2000**, *12*, 222.

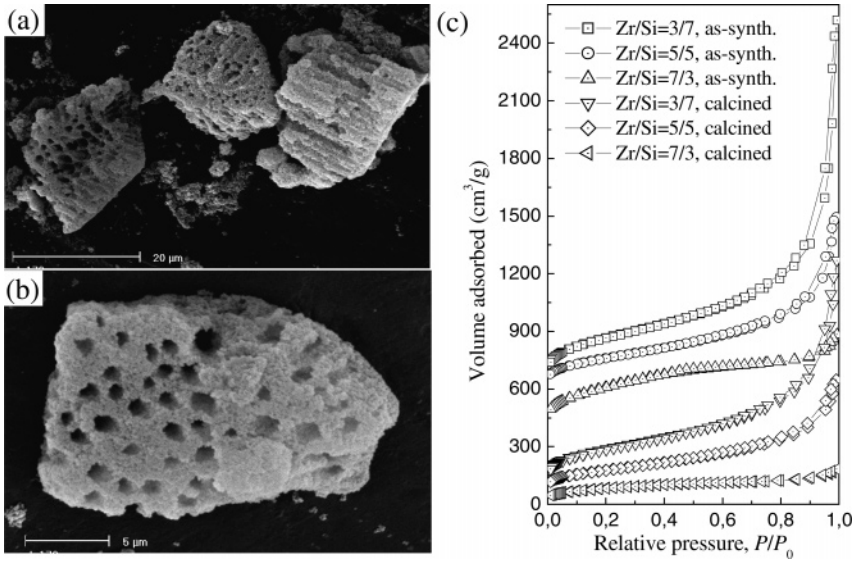

Figure 6. (a, b) SEM images of the meso−macroporous ZS samples with Zr/Si ratio of (a) 3/7 and (b) 7/3; (c) N_2 adsorption−desorption isotherms of the as-synthesized and calcined ZS samples with different Zr/Si ratios, in which the volume adsorbed was shifted by 50, 80, 400, 600, and 600 for the curves of Zr/Si = 5/5, 3/7 in the as-synthesized form and Zr/Si = 7/3, 5/5, 3/7 in the calcined form, respectively.

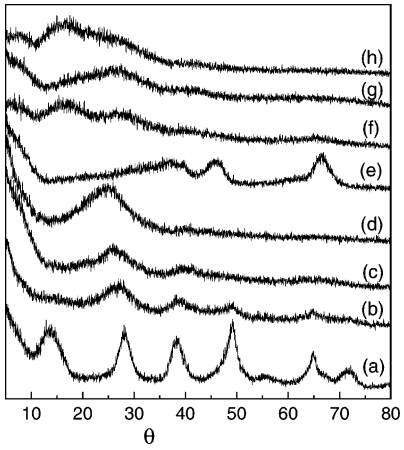

Figure 7. XRD patterns of the as-synthesized meso−macroporous alumina−silica samples with Al/Si ratio of (a) 10/0, (b) 7/3, (c) 5/5, and (d) 3/7. (e−h) Patterns of the calcined samples of parts a−d, respectively.

boehmite to amorphous phase with the increase of the silica content in the samples. Very weak and broad diffraction peaks in the as-synthesized AS with a Al/Si ratio of 7/3 in the synthesis gel might still be assigned to boehmite (Figure 7b). The noncrystalline or amorphous features were presented in the as-synthesized oxides when their Al/Si ratios in the synthesis gel were reduced to 5/5 or lower. Only an XRD broad band at $2\theta = 25-27°$ was observed in the as-synthesized AS with a Al/Si ratio of 3/7 in the synthesis gel, consistent with an amorphous material such as aluminosilicate. The calcined ASs exhibited one to three very weak and broad peaks (Figure 7f−h), which were distinctly different from the γ-Al_2O_3 phase, suggesting the noncrystalline (or semicrystalline) frameworks, since they might match the diffraction patterns of some aluminum silicate coprecipitated mixtures with different silica/alumina ratios, fired to 500 °C.

The BET surface areas and pore volumes of the as-synthesized ASs are quite larger than those of the AlOOH (boehmite), accompanying the larger pore sizes (Table 1). The BET surface areas of the calcined AS samples are smaller than the as-synthesized forms (Table 2) but are still comparative with the surface area of the meso−macroporous γ-Al_2O_3 obtained from the calcination of meso−macrostructured AlOOH. It is quite different when comparing with the case of ZS.

Figure 8 shows the SEM and TEM images of the synthesized AS materials. The uniform macroporous structures with high yields are clearly seen in the monolithic particles. The macropores are mainly 0.8−1.5 μm in size, having a slightly narrower distribution than the meso−macrostructured AlOOH. High-magnification TEM images of the cross-sectional AS specimens also reveal that the macroporous frameworks are amorphous with disordered wormhole-like mesochannels (Figure 8d). There is no fibrous nanoparticle assembly of macroporous frameworks as observed in the meso−macroporous boehmite.[26] These uniform meso−macrostructures of ASs can be preserved after calcination at 500 °C. The macroporous frameworks of the calcined specimens are also the assembly of wormhole-like mesostructured nanoparticles, as revealed by the TEM images.

Only one ^{27}Al NMR signal of octahedrally coordinated aluminum was observed in the as-synthesized aluminum oxide of meso−macroporous boehmite. However, both six- and four-coordinated Al signals were seen in chemical shift ranges of 0−5 and 55−60 ppm, respectively, in the as-synthesized AS samples, and the intensity of the six-coordinated Al signal decreased with the increase of the silica content, accompanying the increase of the intensity of the four-coordinated Al signal (Figure 9). In other words, Al has partly been incorporated in the tetrahedral network with the formation of Al−O−Si bonds in these AS oxides. The ^{27}Al spectra of the calcined samples synthesized with Al/Si ratios of 7/3 and 5/5 contained additional peaks at ~32 ppm, besides the signals of tetrahedral and octahedral Al. The peak at 32 ppm may be due either to pentacoordinated Al or to distorted tetrahedral Al.[29] Pentacoordinated Al species often exist in amorphous aluminosilicates and

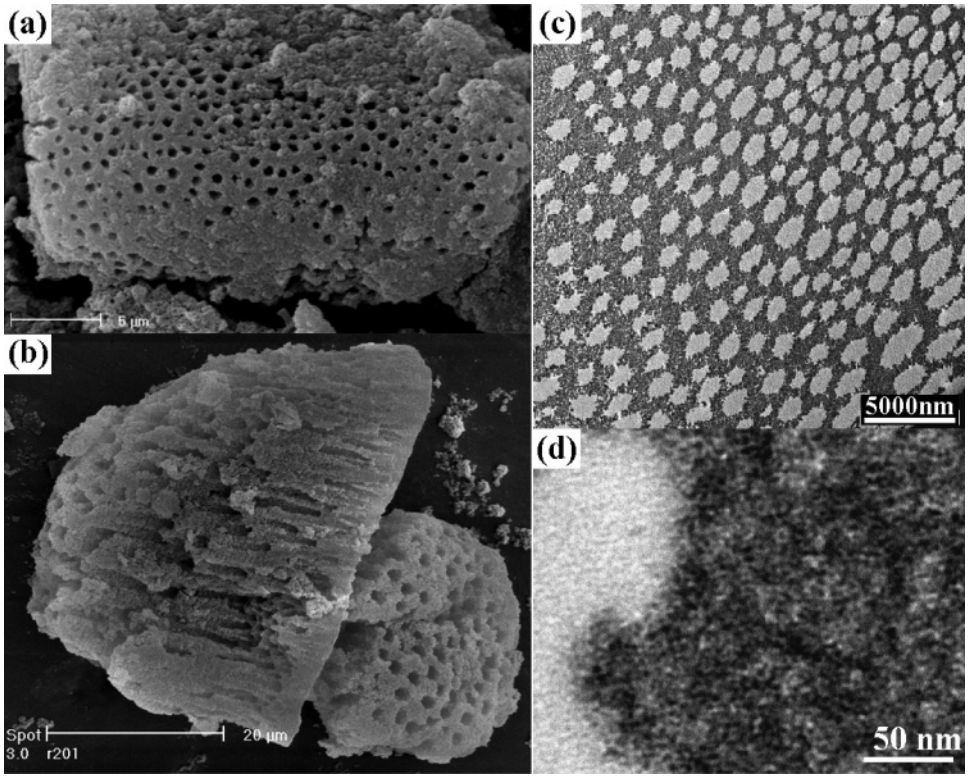

Figure 8. SEM images of the meso−macroporous AS samples with Al/Si ratio of (a) 5/5 and (b) 3/7. (c and d) Low-magnification and high-magnification TEM images of microtomed specimen of the AS sample with Al/Si = 5/5, respectively.

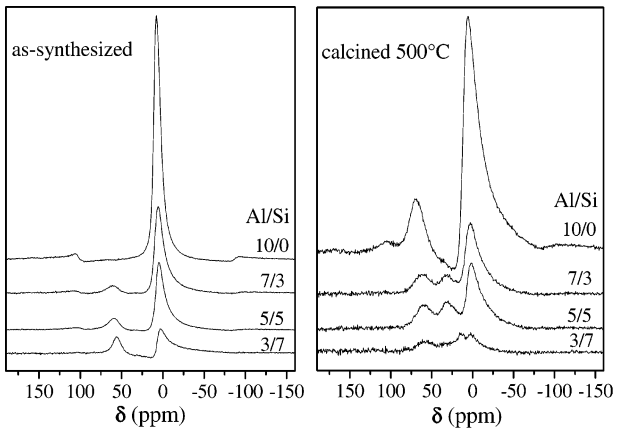

Figure 9. ^{27}Al MAS NMR spectra of the as-synthesized (left) and calcined (right) AS materials with different Al/Si ratios.

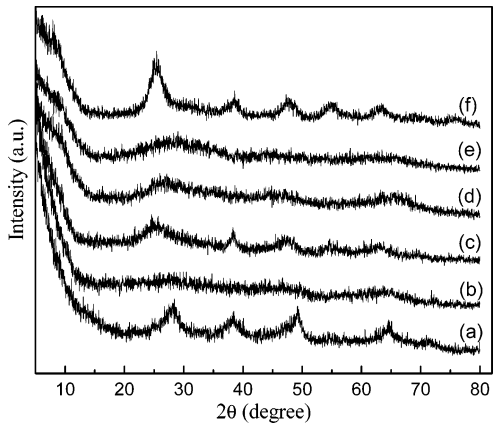

Figure 10. XRD patterns of the as-synthesized meso−macroporous TA samples with Ti/Al ratio of (a) 3/7, (b) 5/5, and (c) 7/3. (d−f) Patterns of the calcined products of parts a−c, respectively.

alumina−silica materials.[29] The calcined sample synthesized with a Al/Si ratio of 3/7 presented an alternative ^{27}Al spectrum with an additional peak at ~15 ppm, and the intensity of this peak was almost the same as that of the six-coordinate Al. Although this chemical shift of 15 ppm is outside the known range for five-coordinated Al in silicates and oxides of about 30 to 40 ppm,[30] it is close to that for trigonal bipyramidal AlO_5 sites best known in $SrAl_{12}O_{19}$, where the isotropic chemical shift has been accurately measured as 18 ppm.[31] Similar signals of ~15 ppm were also detected in $AlPO_4$-21 molecular sieve and $Mg(Si_{0.9}Al_{0.1})O_{2.95}$ perovskite, but their resolutions were poor.[32] It is thus reasonable to tentatively assign this peak as extremely distorted five-coordinated aluminum sites, though more independent evidences are being explored for its unambiguous assignment.

Titania−Alumina. Figure 10 is the XRD patterns of the as-synthesized and calcined TA samples with different Ti/Al ratios. The boehmite phase is predominated in the TAs synthesized with low Ti/Al ratio, while the anatase phase is predominated in the TAs synthesized with high Ti/Al ratio. After calcination at 500 °C,

(29) (a) Schmucker, M.; Schneider, H. *Ber. Bunsen-Ges. Phys. Chem.* **1996**, *100*, 1550. (b) De Witte, B. M.; Grobet, P. J.; Uytterhoeven, J. B. *J. Phys. Chem.* **1995**, *99*, 6961.

(30) Smith, M. E. *Appl. Magn. Reson.* **1993**, *4*, 1.

(31) Jansen, S. R.; Hintzen, H. T.; Metselaar, R.; de Haan, J. W.; van de Ven, L. J. M.; Kentgens, A. P. M.; Nachtegaal, G. H. *J. Phys. Chem. B* **1998**, *102*, 5969.

(32) (a) Jelinek, R.; Chmelka, B. F.; Wu, Y.; Grandinetti, P. J.; Pines, A.; Barrie, P. J.; Klinowski, J. *J. Am. Chem. Soc.* **1991**, *113*, 4097. (b) Stebbins, J. F.; Kojitani, H.; Akaogi, M.; Navrotsky, A. *Am. Mineral.* **2003**, *88*, 1161.

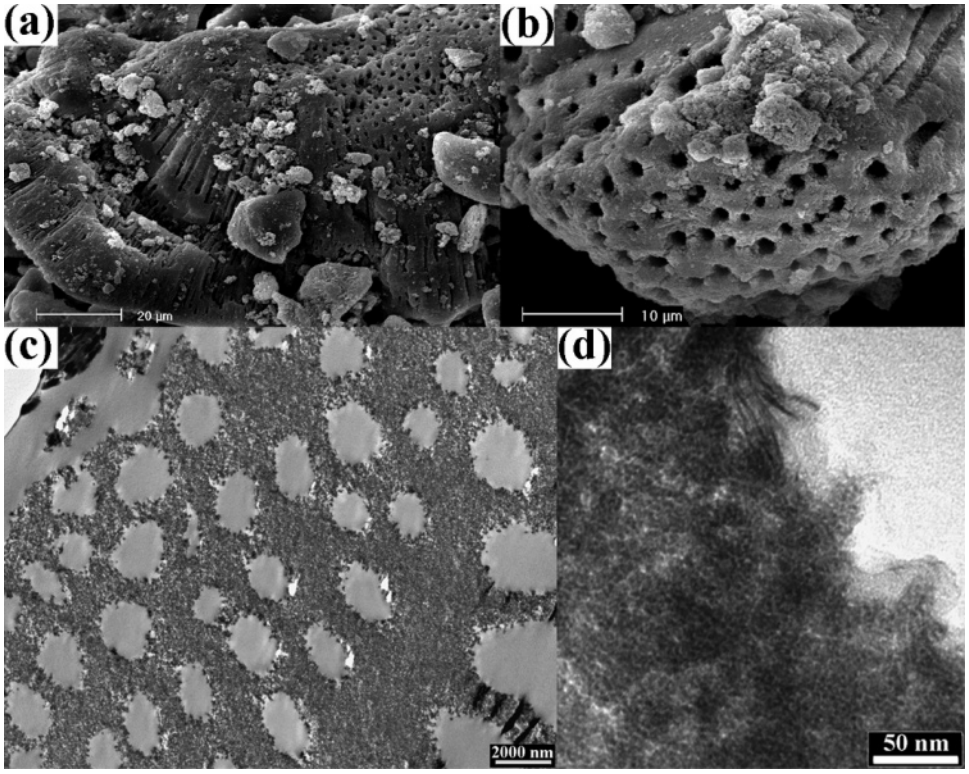

Figure 11. SEM images of the meso−macroporous TA samples with Ti/Al ratio of (a) 3/7 and (b) 5/5. (c and d) Cross-sectional TEM images of the sample with Ti/Al = 5/5.

the samples with high Ti/Al ratio present anatase phase with increased diffraction intensity. The calcined oxides synthesized with Ti/Al ratios of 5/5 and 3/7 are all amorphous. By comparison with the case of AS, both AS synthesized with an Al/Si ratio of 7/3 and TA with a Ti/Al ratio of 3/7, i.e., the main content being alumina with a trace of boehmite phase, can be observed in the as-synthesized forms, but their calcination forms did not present any traces of γ-Al_2O_3 phase, which is the calcination product of boehmite. The possible reason may be the very homogeneous distribution of the Ti and Al components in the TA materials. This could also be supported by the ^{27}Al MAS NMR spectra (Supporting Information). A small content of four-coordinate Al species was seen in all as-synthesized TAs, and the intensity of the six-coordinate Al species corresponded to the content of alumina. Four-, five-, and six-coordinate Al sites were detected in the calcined TA products, which were different from the spectrum of the calcined alumina (γ-Al_2O_3) but similar to the spectra of the calcined ASs.

SEM and TEM images (Figure 11) indicate that the sizes of the macropores are similar to those of the pure aluminum oxides.[26] The high-magnification TEM images reveal that the macroporous walls are composed of wormhole-like mesostructures. Little fibrous nanoparticles can be seen in the macroporous walls, since the crystalline phases of the oxides have been modified in the mixed oxides. This is also consistent with the XRD patterns. The similar wormhole-like mesostructures of macroporous frameworks can still be observed in the calcined forms of TA oxides.

Figure 12 shows the N_2 adsorption−desorption isotherms and the corresponding BJH pore size distribution curves of the as-synthesized and calcined TA samples. All the isotherms of the TAs, whether as-synthesized or calcined, are type IV. The BJH adsorption pore size distribution curves are broadened after calcination, presenting enlarged mesopore sizes in the calcined TAs (Tables 1 and 2). From the high Ti/Al ratio to low Ti/Al ratio, the BJH pore sizes of the TAs decreased, indicating that the mesopore sizes of the TA composites could be tailored by the variation of Ti/Al ratios in the synthesis. The surface areas of the as-synthesized TAs are in the range of 550−900 m^2/g with the pore volumes of 0.89−1.57 cm^3/g. The surface areas of the calcined TAs are in the range of 440−550 m^2/g with pore volumes of 0.94−1.31 cm^3/g. The surface areas of both as-synthesized and calcined TAs are higher than those of meso−macroporous aluminum oxides. Moreover, the calcined TAs have narrower mesopore size distributions than the calcined alumina and titania.

Alumina−Zirconia. Figure 13 is the SEM images of the synthesized AZ samples. The macropore distributions of AZs are not as uniform as those presented in pure aluminas or zirconias. The XRD patterns show the presence of $Al(OH)_3$ bayerite phase in the as-synthesized oxides (Supporting Information). A trace of boehmite could be present when the alumina content was high. After calcination, all AZ samples are amorphous with the absence of any crystalline alumina and/or zirconia phases, showing the composite homogenization of AZs. ^{27}Al NMR spectra contain signals assigned to primarily six-coordinate Al species in the as-synthesized AZs and four-, five-, and six-coordinate Al sites in the calcined products. The intensity of the six- and four-coordinate Al decreased with the decrease of the alumina content in the calcined materials, but the intensity of five-coordinate Al increased.

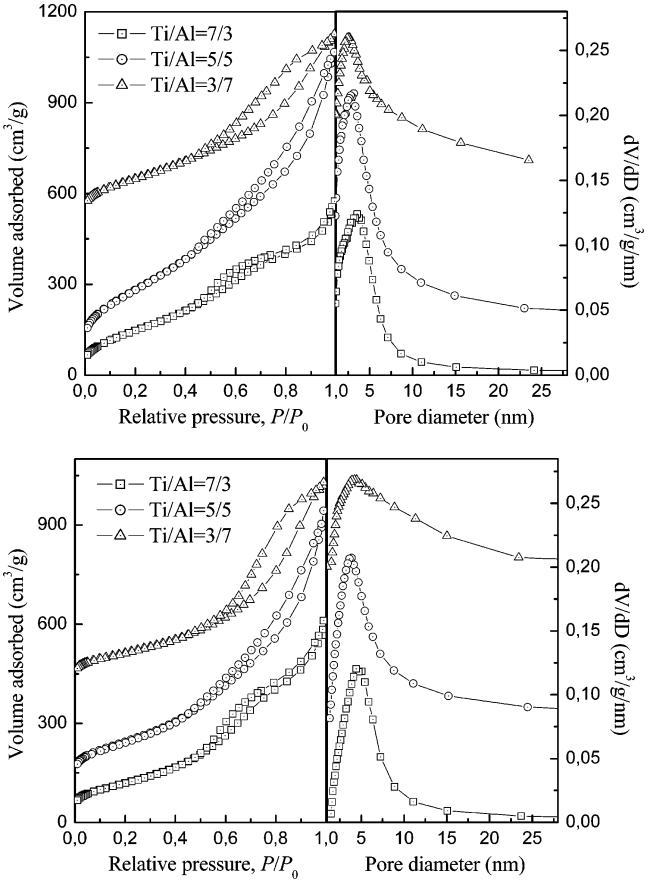

Figure 12. (left) N_2 adsorption−desorption isotherms and (right) the corresponding pore size distributions of the (upper) as-synthesized and (lower) calcined meso−macroporous TA oxides with different Ti/Al ratios. In the as-synthesized materials, the volume adsorbed was shifted by 50 and 500 and the d*V*/d*D* value was shifted by 0.04 and 0.16 for the curves of Ti/Al = 5/5 and 3/7, respectively. In the calcined materials, the volume adsorbed was shifted by 100 and 400 and the d*V*/d*D* value was shifted by 0.08 and 0.20 for the curves of Ti/Al = 5/5 and 3/7, respectively.

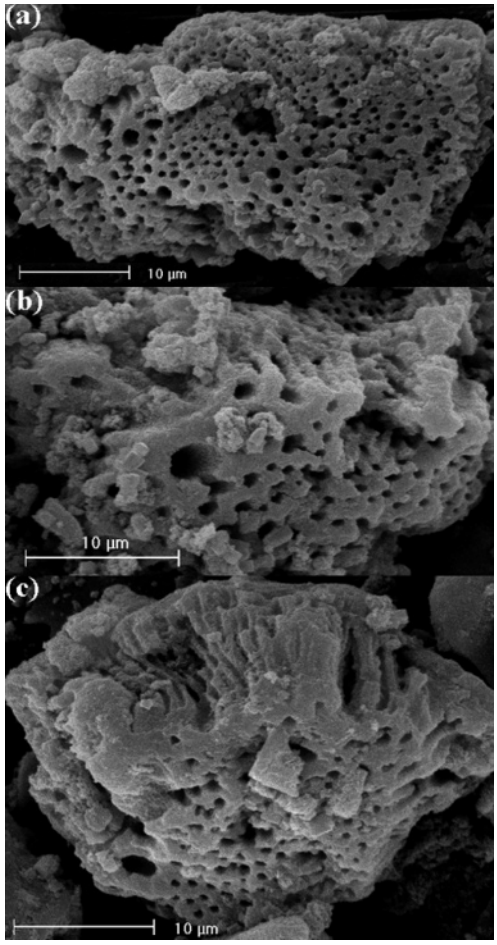

Figure 13. SEM images of the meso−macroporous AZ oxides with Al/Zr ratios of (a) 5/5, (b) 3/7, and (c) 7/3.

Figure 14 shows the N_2 adsorption−desorption isotherms and the corresponding BJH pore size distribution curves of the as-synthesized and calcined AZ oxides. In the part of the isotherms at a relative pressure greater than 0.85, characteristic of the presence of an appreciable amount of secondary porosity,[23] the adsorbed volume of nitrogen increased significantly with the increase of the alumina content, suggesting that the macroporosity could be modified by the Al/Zr ratios. The surface areas of the as-synthesized AZs are larger than 500 m^2/g (Table 1). The mesopore size distributions are quite narrow, with mesopore sizes of ~2 nm. Both the mesopore sizes and the total pore volumes are enlarged with the increase of the alumina content. After calcination at 500 °C, the surface areas are reduced to 300 m^2/g or so (Table 2), which are smaller than that of the meso−macroporous γ-Al_2O_3 but still much larger than that of the calcined zirconia.

Discussion

In the preparation of multicomponent systems, it is essential to promote cohydrolysis of the mixed alkoxides with a similar rate, to ensure a homogeneous distribution of the components at a molecular, or at least nanometrical, scale. During the present synthesis, cohydrolysis of mixed alkoxides occurs to produce $(M_A,M_B)O_2$ species, and the primary nanoparticles of mesostructured surfactant/$(M_A,M_B)O_2$ composites, which are considered to be homogeneous, are formed with a large number of surface hydroxyl groups due to incomplete condensation. On the basis of a series of experimental results realized in the presence and absence of surfactant molecules, it was found that no macrochannels were observed if the synthesis was carried out with a long period of stirring without the presence of surfactant, and materials with macropores synthesized in the presence of surfactant could have a higher surface area.[33] Thus, we originally suggested that the surfactant molecules in solution could be regarded as the directing agent of an ordered array of macrochannels through the formation of supermicelles.[23] Recently, this mechanism became the point of debate in the light of the new studies. Mann et al.[34] reported that a similar macroporous structure of titania was obtainable in ammonia solution in the absence of auxiliary organic templates without stirring. In our present case, the preparation of hierarchical meso−macroporous structures was performed in acid solution with stirring. Comparing our previous and present results with those reported by Mann et al.,[34] it

(33) Blin, J. L.; Gigot, L.; Leonard, A.; Su, B. L. *Stud. Surf. Sci. Catal.* **2002**, *143*, 1035.
(34) Collins, A.; Carriazo, D.; Davis, S. A.; Mann, S. *Chem. Commun.* **2004**, 568.

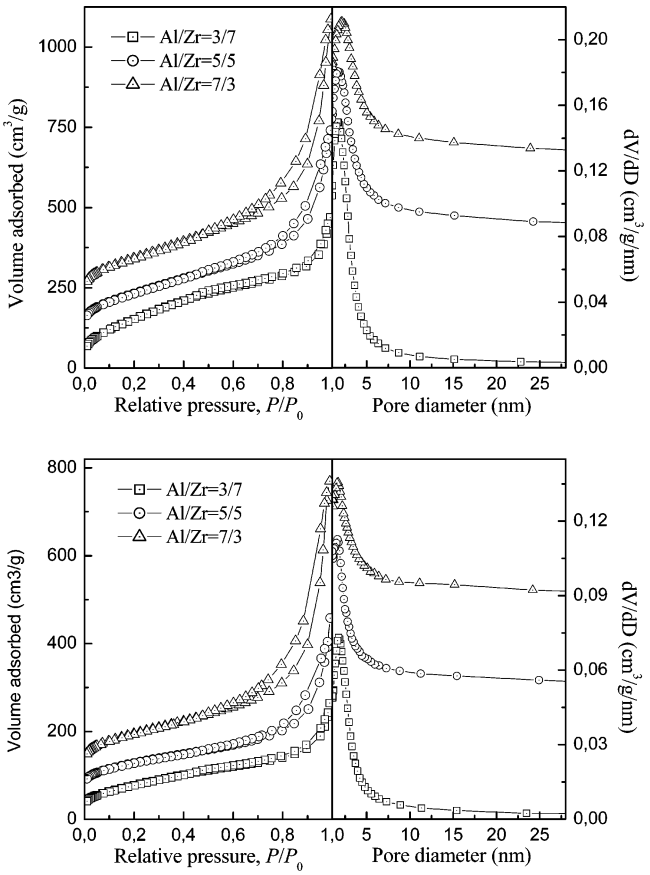

Figure 14. (left) N_2 adsorption−desorption isotherms and (right) the corresponding pore size distributions of the (upper) as-synthesized and (lower) calcined meso−macroporous AZ oxides with different Al/Zr ratios. In the as-synthesized materials, the volume adsorbed was shifted by 100 and 200 and the d*V*/d*D* value was shifted by 0.08 and 0.12 for the curves of Al/Zr = 5/5 and 7/3, respectively. In the calcined materials, the volume adsorbed was shifted by 50 and 100 and the d*V*/d*D* value was shifted by 0.05 and 0.08 for the curves of Al/Zr = 5/5 and 7/3, respectively.

seems that the stirring can also play a role in the formation or not of the macrochannels. This is a quite complex system, and a further investigation by a multiple technique approach is still being done to clarify the different key factors of the synthesis mechanism.

The most important criteria for the preparation of mixed metal oxide materials are the homogeneity of the different components and control of the final metal-to-metal ratio. The use of mixed alkoxide solutions and surfactants allows the formation of binary metal oxide materials with structural properties of large multiporosity and high specific surface area, and an improved catalytic efficiency could be expected for these meso−macroporous binary metal oxide composites due to both the presence of a secondary metal oxide and structural control. In these meso−macroporous materials of TZ, ZS, TA, AS, and AZ, the presence of the second component in sufficient amounts is obviously inhibiting crystallization and the consequent structural growth, resulting in higher surface areas, as well as the controlled pore sizes. This has been supported by XRD, N_2 adsorption analysis, solid-state NMR spectroscopy, and electron microscopy. The XRD data revealed the presence of both anatase and brookite phases in the as-synthesized titania network and boehmite phase in the as-synthesized AlOOH. The mixing of zirconia, silica, and alumina with titania resulted in the disappearance of the brookite phase and the noncrystallization of the framework structure in the synthesis with the increase of the secondary oxide content. A similar case also took place for the alumina-based binary oxides. After calcination at 500 °C, the pure titania, zirconia, and alumina exhibited anatase and brookite, tetrahedral ZrO_2, and γ-Al_2O_3, respectively, while the binary oxides were either bicrystalline with low crystallinity, noncrystalline, or amorphous. This suggests that the mixing of secondary oxides could inhibit the crystallite growth not only during the synthesis but also upon heat treatment and make the materials more stable against the phase transformations (for example, anatase-to-rutile, boehmite-to-γ-Al_2O_3, amorphous-to-tetrahedral ZrO_2) upon calcination. Thus the amorphous structure is observed in the calcined AS, ZS, TA, and AZ composites instead of crystalline phases. Consequentially, thermally stable binary oxides could be obtained with higher surface areas than the single metal oxides.

Good homogeneity has been seen in the synthesized meso−macroporous binary metal oxides, since the homocondensation of the precursors for the formation of M_A−O−M_A and M_B−O−M_B can guarantee the good distribution of two metal oxides in one solid body and can also induce the formation of some M_A−O−M_B bonds. Both four- and six-coordianted Al species were in the as-synthesized AS and TA materials, while only one ^{27}Al NMR signal of octahedrally coordinated aluminum was observed in the as-synthesized aluminum oxide. Moreover, the intensity of the four-coordinated Al signals increased with the content of silica (Figure 9). Five-coordinated Al existed in all calcined products of AS and TA, which was not present in the calcined alumina. ^{29}Si and ^{27}Al MAS NMR spectra evidently provided that a small quantity of Al has been incorporated in the tetrahedral network with the formation of a few of Al−O−Si bonds in the AS oxides and the formation of Al−O−Ti bonds in the TAs. On the other hand, the nature of the secondary oxides would also affect the crystalline phases of the resultant binary oxide materials. In the alumina-based binary oxides, traces of boehmite phase could still be seen in the as-synthesized TAs and ASs with high content of alumina, although the diffraction peaks were quite weak and broad, but the bayerite phase was present in the as-synthesized AZs. This might be due to the existence of the interaction between Al and Zr species during the synthesis. The calcined AZs were amorphous, and no crystalline ZrO_2 phases were observed, despite the high content of zirconia, which is quite different from the case of TZs. The possible cause for this difference is the different interaction chemistry between Ti and Zr, and Al and Zr precursors, and thus the formation of a few of Ti−O−Zr and Al−O−Zr bonds could be reasonably deduced. The formation of some M_A−O−M_B bonds is indirect evidence of the homocondensation of different metal oxide precursors.

One new feature of the current synthesis methodology for the hierarchical binary oxides having a bimodal meso−macroporous structure is using the mixed alkoxide precursors without the need of the polymer latex spheres usually reported as the template to create the

uniform macropores. The addition of salts or cosurfactants or cosolvents is also not needed. Both the macropore and mesopore sizes could be tailored by the variation of the M_A/M_B molar ratios, as well as the high surface areas and pore volumes. Stucky et al. once prepared some mesoporous mixed oxides such as $SiAlO_y$, Al_2TiO_y, $SiTiO_y$, and ZrW_2O_y by using inorganic salts and a triblock copolymer; however, all of them were amorphous with low surface areas.[11] Our present meso−macroporous binary oxides have tunable porosities and very high surface areas with (semi-)crystalline channel walls, which should be significant and can find practical applications in multiple fields.

Conclusions

The hierarchically meso−macrostructured binary mixed oxides of various components with a macroporous framework composed of accessible and interconnected wormhole-like mesopores have been synthesized by a very simple process. The macropores are in one-dimensional orientation, parallel with each other. Almost all binary oxide composites have higher surface areas and larger pore volumes than single metal oxides. These binary oxides exhibit different crystalline phases of network materials in comparison with their analogues of single oxides, indicating that the addition of a secondary oxide results in the crystal modification. The mesopore sizes of the binary oxides, as well as macropore sizes, could be tailored by the variation of the composition contents. The thermal stabilities of the binary oxide composites are higher than single metal oxides. The multiscaled pore sizes and a wide variety of chemical compositions were integrated into modulable monolithic materials, which should be promising for multiple applications in catalysis and separation technology.

Acknowledgment. This work was realized in the frame of Belgian Federal Government PAI-IUAP 01/5 and financially supported by the European Program of InterReg III (Program France-Wallonie-Flandre, FW-2.1.5).

Supporting Information Available: XRD, N_2 adsorption analyses, SEM and TEM images, and solid-state NMR spectra of the macro−mesostructured binary oxide compositions. This material is available free of charge via the Internet at http://pubs.acs.org.

CM0494812